JOURNAL OF GEOPHYSICAL RESEARCH, VOL. 107, NO. A8, 1167, 10.1029/2001JA900102, 2002

Particle simulations of relativistic electron beam injection from spacecraft

Torsten Neubert
Danish Space Research Institute, Copenhagen, Denmark

Brian E. Gilchrist
Space Physics Research Laboratory, University of Michigan, Ann Arbor, Michigan, USA

Received 1 April 2001; revised 27 June 2001; accepted 27 June 2001; published 6 August 2002.

[1] Linear accelerators producing relativistic (5 MeV) electron beams are now down to a size that allows them to be flown on spacecraft and sounding rockets. This opens up new opportunities for atmospheric/ionospheric modification experiments where the mesosphere and lower thermosphere regions can be perturbed down to 40-km altitude. In this paper the relativistic electron beam injection process is investigated by means of three-dimensional particle-in-cell simulations to determine the initial interaction of the beam with the spacecraft and the ambient plasma. The results indicate that relativistic beams are more stable than keV-energy beams investigated in the past, allowing the injection and propagation of beams with currents several orders of magnitude higher than those for keV-energy beams. The superior stability of relativistic beams is the result of a combination of effects including the higher relativistic electron mass, a lower beam density, and a smaller effect from spacecraft charging. Relativistic beams injected downward from spacecraft are therefore expected to deposit a large fraction of the energy in the middle atmosphere. In the high-current limit ($I > 100$ A) the beam self-fields are strong. In this regime a beam may propagate in the ion-focused regime, where beam electrons expel ambient electrons to create a channel of ambient ions that space charge neutralize the beam. The establishment of the ion channel, however, creates significant turbulence and scattering. *INDEX TERMS:* 2403 Ionosphere: Active experiments; 2494 Ionosphere: Instruments and techniques

1. Introduction

[2] When it was realized that relativistic beam accelerators (5 MeV) could be flown on spacecraft, studies were undertaken to investigate the use of such beams for atmospheric modification experiments [*Banks et al.*, 1987, 1990]. The primary attraction was the prospect of a new technique to explore a region of the atmosphere difficult to study by in situ observations. The applications discussed in these reports included investigations of the fair weather electric field and studies of chemical reaction path changes by relativistic electron precipitation. With the later discovery of electric discharges in the mesosphere above severe thunderstorms (sprites) [*Sentman et al.*, 1995], it was further suggested that relativistic beams injected over thunderstorms could trigger artificial upward discharges [*Neubert et al.*, 1996].

[3] Following these initial studies, large-scale models of beam propagation were developed to predict the level of perturbation of the atmosphere [*Neubert et al.*, 1996] and the ionosphere-magnetosphere [*Khazanov et al.*, 1999, 2000]. In order to provide more realistic estimates of the initial conditions of beam parameters for the large-scale models, the three-dimensional (3-D) particle-in-cell (PIC) simulations of the beam injection process presented here were undertaken. The question to be addressed is to what extent spacecraft charging and beam plasma interactions affect beam coherence during the initial stage, where the beam propagates from the beam accelerator, through the spacecraft potential sheath, and into the ambient plasma.

[4] The typical performance values of linear accelerators (linacs) that can be flown today are as follows: beam current, $I_b = 0.1$ A, energy $E_b = 5$ MeV, pulse length $\tau_b = 4$ μs, duty cycle $T_d = 0.001$, radius at the accelerator exit $a_o = 1.5$ mm, and density at the accelerator exit $n_b^o = 2.9 \times 10^{14}\mathrm{m}^{-3}$. With the above parameters, the average current is $I_{av} = T_d I_b = 0.1$ mA. The quality of a beam (coherence) can be characterized by the normalized beam emittance ϵ_n [*Lawson*, 1988]. For the linacs considered here, $\epsilon_n = 0.018$ cm-rad. See the work of *Jost* [1993] for more technical details.

[5] It was soon discovered from initial test runs that relativistic beams are much more stable than keV-energy beams studied in the past [*Neubert and Banks*, 1992] and that microsecond-duration pulses with the above characteristics at least initially would propagate with a high degree of stability. During single-pulse injections, the condition simulated here, the effects of spacecraft charging or beam plasma interactions were seen to become important only for

0148-0227/02/2001JA900102

currents of the order of 100 A or more. As a consequence, this study focuses on high-current beams, which are likely not practical for present-day technology but perhaps will be in the future. This regime may also be of interest to studies of sprites and their interaction with the ionospheric plasma, where theory and observations suggest that electrons may be accelerated to relativistic energies and be injected from the atmosphere and into the magnetosphere [*Lehtinen et al.*, 2000].

[6] Scaling of parameters from the real world to PIC simulations is often an issue. While the scaling of most aspects is done in a self-consistent manner in the simulations presented here, not all of the system can be simulated properly, owing to the lack of spatial resolution on a 3-D grid. To improve the resolution of the simulation box, shorter pulses of 1-μs duration are simulated rather than the longer pulses of the linac mentioned above. In addition, a relatively higher magnetic field is imposed to limit the beam gyroradius. The impacts of these assumptions are minor and are discussed in the following sections. However, to strengthen the case, the stability of MeV beams relative to keV beams is further demonstrated by repeating the simulations with keV-energy beams.

[7] The simulations are performed using the Tridimensional Stanford (TRISTAN) electromagnetic and relativistic particle code [*Buneman*, 1993]. The code uses local updates of the fields from particle motions, rather than Poisson's equation. While this scheme makes the code fast, it is required that the experimental conditions are described self-consistently within the simulation domain.

2. Simulation Parameters

[8] The scaling of spacecraft charging from the real world to the simulations is done by following the normalized potential Φ:

$$\Phi = \frac{qV}{mc^2}, \tag{1}$$

where V is the spacecraft electric potential. The self-consistent implementation of a spacecraft in the TRISTAN code and the appropriate scaling laws are described in some detail by *Neubert and Gilchrist* [2002]. Here we just outline some general considerations behind proper scaling of the system.

[9] Beam experiments in space and related beam simulation studies of the past considered beam pulses with pulse lengths of the order of milliseconds or more [*Neubert and Banks*, 1992]. Studying microsecond-duration pulses corresponds to investigating the beam front in these experiments. A key parameter describing the charging state during pulse emissions is the plasma response time τ_p, which is of the order of $1/f_p$. The ambient plasma density for which $\tau_p = \tau_b = 1$ μs is $n_p = 2.7 \times 10^{10}\mathrm{m}^{-3}$. For comparison, f-peak ionospheric densities typically range from 10^{10} (night) to $10^{12}\mathrm{m}^{-3}$ (day), or $\tau_b/\tau_p = 0.9$ to 9.

[10] In the ionosphere, steady state charging conditions are then expected to be approached during a pulse emission. Regions of low plasma density are found both below and above the ionosphere. Below the ionosphere the beam-spacecraft system is dominated by collisional interactions with the atmosphere, which lead to the creation of a substantial flux of secondary electrons [*Neubert and Banks*, 1992], a regime not considered here. However, well above the ionosphere, in the magnetosphere, the plasma density may be so low as to create conditions where steady state is not reached.

[11] From the above discussion it is clear that the first parameter to scale properly in the simulation is the ratio of the beam pulse time to the plasma response time. This scaling is also needed for the correct simulation of beam-plasma interactions. In the simulations, two situations will be studied. One is pulse injection into a vacuum, representing magnetosphere injections from a satellite into a thin ambient plasma, and the other is injection into a plasma with several ambient plasma periods during one beam pulse duration, representing ionospheric injections. In these two limits, the precise pulse length is not of importance, and the simulations can be taken to represent the injection of the 4-μs duration linac pulse.

[12] A second process to scale properly is the charging experienced by a spacecraft during a pulse injection. The charging rate, if large, may severely affect the beam pulse escape energy from the spacecraft sheath and modify the beam dynamics. The charging rate of a conducting sphere in vacuum is $dV/dt = I/C$, with $C = 4\pi\epsilon_o r$, where V is the voltage, I is the current, C is the capacitance, and r is the radius of the sphere. With an equivalent spacecraft radius of $r = 1$ m, $I_b = 1$ A, and $\tau_b = 1$ μs, the charging during a single-pulse injection is 9 kV, which is small relative to a beam energy of 5 MeV.

[13] During extended series of pulse emissions, the average injected beam current is 0.1 mA. In the ionosphere the thermal current density is of the order of 1 mA m^{-2}, and spacecraft charging in the ionospere will therefore not be a concern for present-day accelerators. In the magnetosphere, however, charging effects must considered.

[14] To get into an interesting regime during a single-pulse injection, one may then attempt to simulate accelerator systems of the future with either longer beam pulses or higher currents. In the present study we chose to investigate the case of higher currents, as beam stability also depends on the beam electron density and current. In addition, shorter beams lend themselves better for simulations, as mentioned earlier.

[15] The simulation domain is on a 3-D grid with grid spacing $\Delta = 1$ and time step $\Delta t = 1$. The velocity of light $c = 0.5$, such that a relativistic electron will move $\sim 0.5\Delta$ in one time step. The simulation grid used is $1024\Delta \times 64\Delta \times 64\Delta$, with the beam pulse propagating in the positive x direction. The pulse is assumed to be of 1-μs duration, which brings it into the regime of several plasma periods per pulse for ionospheric conditions. The pulse duration is chosen to be $1000\Delta t$, which allows both the head and tail of the pulse to be resolved properly. This means that Δ in the simulation is equivalent to 0.6 m in the real world for the 5-MeV beam.

[16] The spacecraft is as a cube of size $10\Delta \times 10\Delta \times 10\Delta$, centered in y and z and at $x = 64\Delta$, such that the approximate equivalent spherical spacecraft radius is $r = 5\Delta$. The spacecraft radius is then equivalent to 3 m, which is on the large side for a sounding rocket or spacecraft in the ionosphere.

Table 1. Simulation Parameters and Correspondence With Real World Currents and Densities

	$\gamma - 1$	N^+	n_b^o/n	Φ	I, A	n_b, m^{-3}
Sim 1	9.8	10	2.3	0.5	84	10^{12}
Sim 2	9.8	100	23	5	840	10^{13}
Sim 3	0.1	1	0.5	1	8.4	2.3×10^{11}
Sim 4	0.1	10	5.2	–	84	2.3×10^{12}

[17] The ambient simulation density is $n = 1.6$, which is a low number to reduce computational effort but not too low to resolve kinetic plasma effects. The plasma frequency is chosen to have ~6.5 ambient plasma periods during one beam pulse injection. The magnetic field is directed along the x axis with a strength such that the relativistic gyrofrequency is about one third of the plasma frequency. This somewhat large magnetic field for ionospheric conditions is needed to limit the beam expansion in the y and z directions and thus limit the volume of the simulation domain. The effect is to overestimate the beam density, as discussed further in section 5.

[18] In the simulation, ions are assumed to be stationary as the physics simulated is on a timescale of a few tens of electron plasma periods. With the TRISTAN code, one need not include ions at all in this case, because electric fields are directly updated from particle currents, thus further reducing the computational load.

[19] The effective beam accelerator radius (after smoothing of particles) is a little over 1Δ, corresponding to ~0.8 m in the real world. This means that the simulations do not have the resolution to follow the initial expansion of the beam. However, beam expansion being important, the longer-scale expansion is discussed extensively in section 3. For the relativistic beams the simulated energy is 5 MeV, or $\gamma - 1 = 9.8$, and the number of particles injected per time step is chosen to be $N^+ = 10$, 100. The ratios of the beam and plasma densities at the accelerator are $n_b^o/n = 1.9$ and 19, respectively. The parameters $q = 3.25 \times 10^{-2}$, $m_e = 1$, and $B = 3.69$ are chosen such that the plasma and gyrofrequencies have the values given above and the beam current is of a magnitude that brings the normalized spacecraft potential Φ to 0.5 and 5 at the end of a pulse injection into vacuum, thus simulating the low- and high-charging regime.

[20] The correspondence between the currents simulated and real currents can be estimated from the analytical charging calculation of section 1. With the equivalent spacecraft radius of 3 m and the pulse duration of 1 μs, the corresponding currents are 84 and 840 A. An independent check of consistency can be made from a comparison of beam densities at the simulation accelerator exit. When a real beam has expanded to a radius of 0.8 m, which is the approximate beam accelerator radius in the simulations, the beam densities are of the order of 10^{12} and 10^{13} m^{-3}. The ratios of beam density to typical ionospheric densities are then consistent with values of n_b^o/n used in the simulations.

[21] For the keV beams the energy simulated is 50 keV, where $\gamma - 1 \simeq 0.1$ and $\beta = v_b/c = 0.44$. Because of spacecraft charging effects, lower currents are simulated

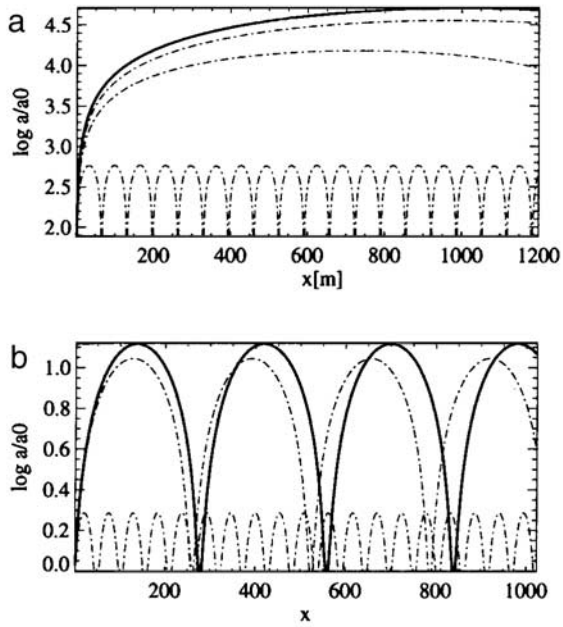

Figure 1. Envelopes of 5-MeV-energy beams for different currents. (a) Real beams, I_b = 1, 30, 60, and 100 A. The thick curve represents all nonneutralized beams ($f = 0$) since K^o is small for the current values investigated. It also represents the neutralized case ($f = 1$) at the lowest current value, where K^1 also is small. The dashed curves are for neutralized beams with I_b = 30, 60, and 100 A, where increased currents have increased pinching effect on the beam. (b) The same for simulated beams with N^+ = 1, 10, and 100. The modulation of the thick curves reflects magnetic field-induced modulations, which are relatively faster in the simulations.

Table 2. Magnitude of Terms in Equation (2) for 5-MeV Beam Injection in the Ionosphere With Magnetic Field B = 56,000 nT and in the Simulation

I_b	$0{:}K^o/a_o$	$1{:}K^1/a_o$	$2{:}\varepsilon^2/{a_o}^3$	$3{:}(\Omega_L^2/\beta^2c^2)a_o$	$a/a_o1 = 2$	$a/a_o2 = 3$	$a/a_o1 = 3$
			Real World, B = 56,000 nT				
10 A	6.3×10^{-4}	-7.3×10^{-2}	9.6	3.6×10^{-9}	11	227	4,485
100 A	6.3×10^{-3}	-7.3×10^{-1}	9.6	3.6×10^{-9}	3.6	227	14,1831
1,000 A	6.3×10^{-2}	−7.3	9.6	3.6×10^{-9}	1.1	227	14,183
			Simulation				
$N^+ = 10$	1.1×10^{-5}	-1.2×10^{-3}	1.7×10^{-2}	1.2×10^{-4}	3.7	3.4	3.1
$N^+ = 100$	1.1×10^{-4}	-1.2×10^{-2}	1.7×10^{-2}	1.2×10^{-4}	1.2	3.4	10

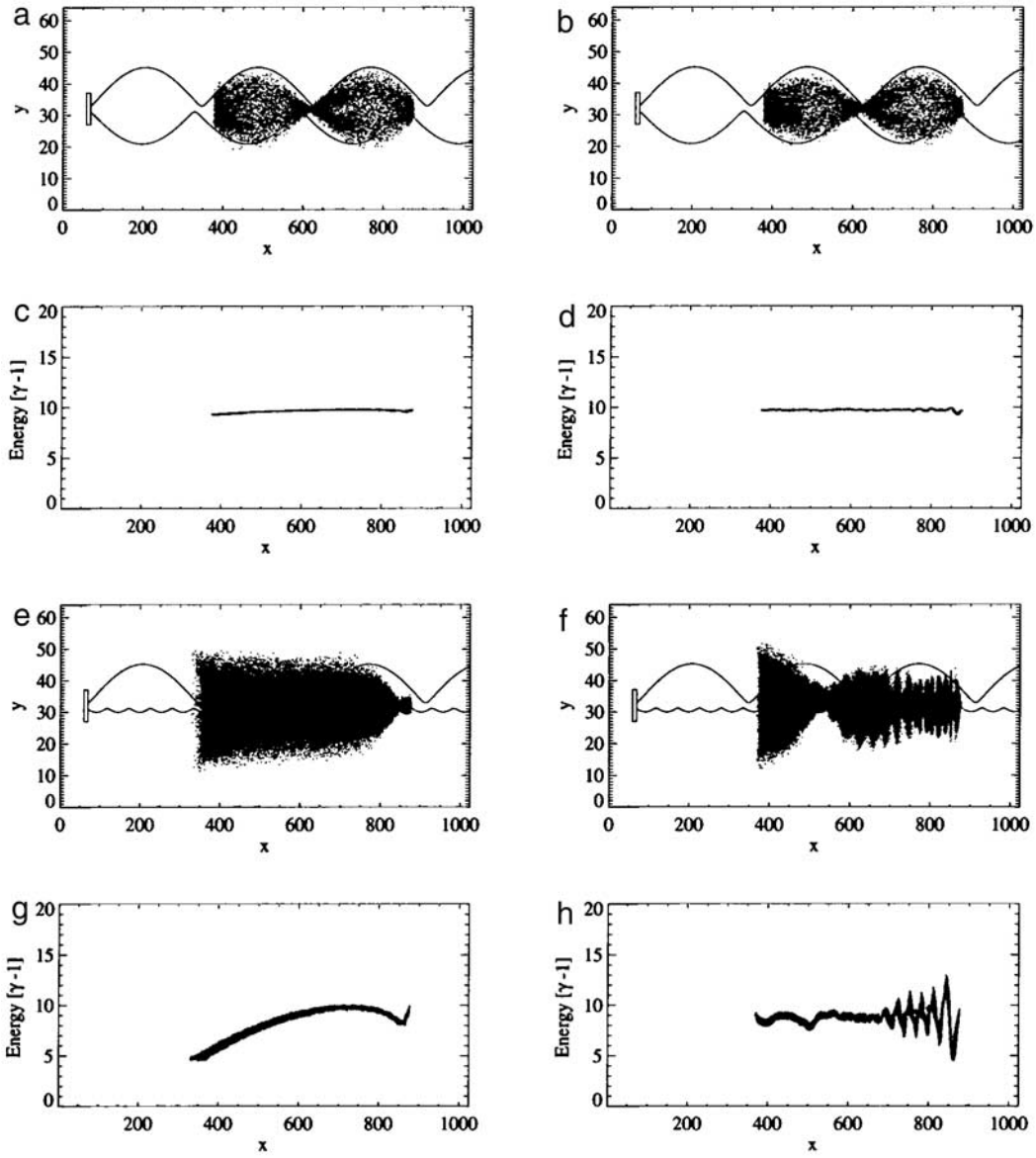

Figure 2. (a–h) Electron beam with energy 5 MeV injected into a (left) vacuum and (right) plasma at time $t = 1624\Delta t$. In Figures 2a–2d the beam current is $N^+ = 10$, corresponding to a beam density at the accelerator $n_b^o = 3$. In Figures 2e–2h the beam current is $N^+ = 100$, corresponding to a beam density at the accelerator $n_b^o = 30$. The ambient plasma density is $n = 1.6$. The magnetic field is directed along x with $\Omega_L \Delta t = 5.610^{-3}$. The beam pitch angle at injection $\theta = 0°$, with $\Delta\theta = 8°$. The beam pulse length $t = 1000\Delta t$. The horizontal scale is highly compressed (8 times) as seen in the distortion of the spacecraft, which is really in the shape of a cube. The curves are the solutions to the beam envelope equation (2), where the top curve is for a nonneutralized beam ($f = 0$) and the bottom curve is for a neutralized beam ($f = 1$).

with $N^+ = 1, 10$. It is noted that the full beam pulse for $N^+ = 10$ is not able to escape the spacecraft in vacuum. Table 1 summarizes the parameters for the beams.

3. The Envelope Equation

[22] It is important to understand the radial expansion of the beam, because the stability of the beam in the plasma depends on the ratio of the beam and the ambient plasma density. In the limits of either low or high relative beam density, the interaction is weak.

[23] The radial expansion of a beam is described by the paraxial envelope equations [*Lawson*, 1988; *Humphries*, 1990]. Considering only terms relevant for the present problem of a relativistic electron beam in a magnetic field, the equations reduce to

$$a'' = \frac{K}{a} + \frac{\epsilon_n^2}{a^3} - \frac{\Omega_L^2}{\beta^2 c^2} a, \tag{2}$$

where a'' is the second derivative of the beam radius with respect to the distance along the beam axis and

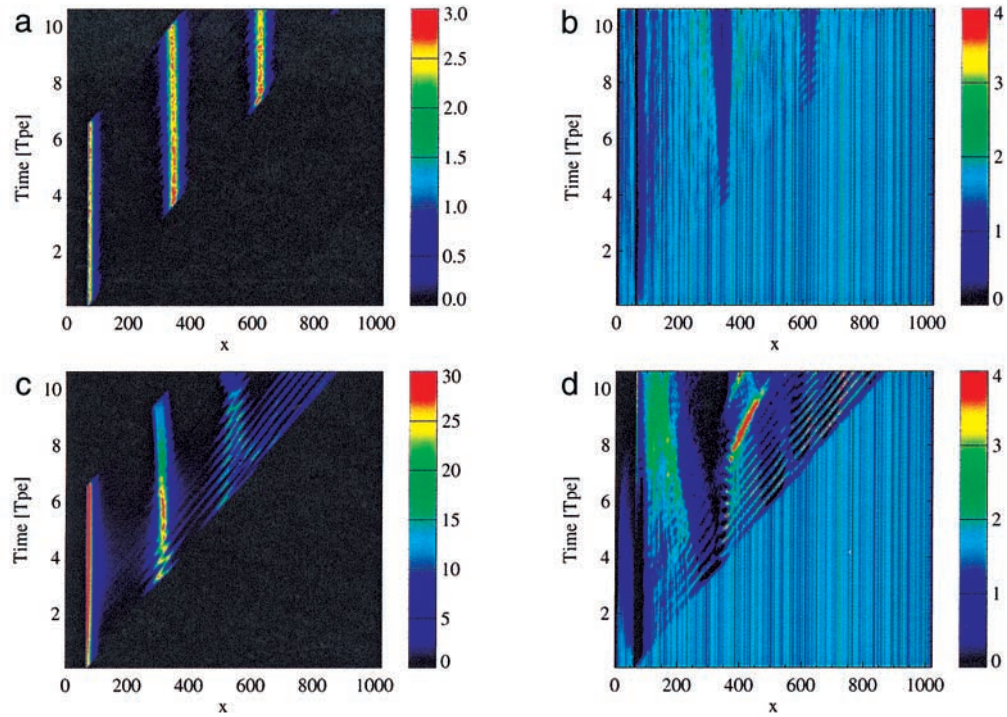

Figure 3. (a, c) Beam density and (b, d) ambient plasma density on the beam axis as a function of time and position along x. The beam energy is 5 MeV. The beam currents are $N^+ = 10$ (a, b) and $N^+ = 100$ (c, d). Other parameters are as in Figure 2.

$\Omega_L = -qB/2\gamma m_o$ is the beam electron Larmor frequency. K is the generalized perveance:

$$K = \frac{2I}{\beta^2\gamma}\left(\frac{1}{\gamma^2} - f\right), \tag{3}$$

where the normalized current $I = I_b/I_o$ and

$$I_o = \frac{4\pi\epsilon_o m_o c^3}{q} (= 17,000\text{A}). \tag{4}$$

[24] The perveance is the sum of beam-generated forces from the nonneutralized space charge within the beam, which attempts to expand the beam, and the beam self-magnetic field, which tends to contract the beam. The parameter f is the degree of beam charge neutralization by the ambient plasma, and it takes on values between 0 and 1. A completely charge-neutralized beam will have $f = 1$, in which case K is negative. It is interesting to look at the perveance values in the limits $f = 0$, 1 for nonrelativistic ($\gamma = 1$) and relativistic ($\beta = 1$) beams. At these limits we have the following:

Nonrelativistic

$$-2I < K < 2I/\beta^2, \tag{5}$$

Relativistic

$$-2I/\gamma < K < 2I/\gamma^3. \tag{6}$$

[25] For nonrelativistic beams, K is more likely to be positive, while for relativistic beams, K will often be negative. From (2) one can see that the sign of K is important for the propagation characteristics. Even with no ambient magnetic field, relativistic beams with K negative have the possibility of propagation with the radius maintained below a maximum value. In this case the positive emittance term balances the negative perveance term. Moving to relativistic beams, one then has to consider the new phenomena of beam propagation in the ion-focused regime.

[26] To better understand the relative importance of the three terms in the envelope equation, and to help assure that they are scaled properly in the simulations, values of the terms at injection are computed for beam currents from 10 to 1000 A for the beam radius at the accelerator exit $a_o = 1.5$ mm as assumed for the linac. The values are also determined for the simulations of 5-MeV beams, using $a_o = 1\Delta$. In addition, the beam radii for which the terms become of equal magnitude have been calculated, for instance, the value for which term 1 equals term 2. The results are shown in Table 2, which shows the perveance term for the two cases of $f = 0$ (K^o) and $f = 1$ (K^1).

[27] First it is noted that the emittance term, in general, dominates. It can be shown that in this case the beam initially expands with the emittance angle $\Theta_e = \epsilon/a_o$, where the emittance $\epsilon = \beta\gamma\epsilon_n$. In the case of a charge-neutralized beam the next term to dominate when the radius increases is the perveance term. Finally, if the beam continues to expand, the ambient magnetic field will eventually reduce the radius again.

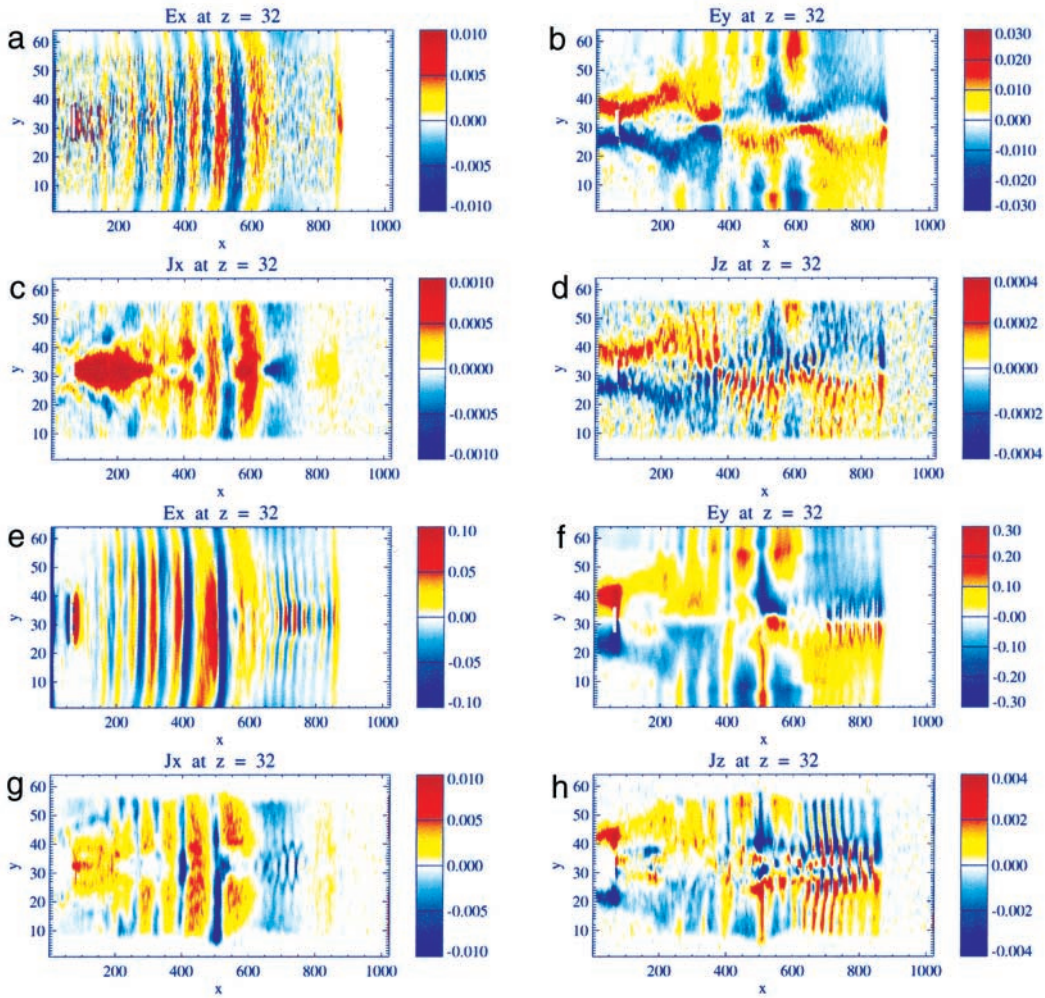

Figure 4. Electric field x, y components and ambient plasma current density x, z components in the xy center plane at time $t = 1624\Delta t$. The beam energy is 5 MeV. (a–d) $N^+ = 10$. (e–h) $N^+ = 100$. Other parameters are as in Figure 2.

[28] In the simulations the relative ordering of the terms is maintained from the real world with the exception that the magnetic field focusing term (3) is somewhat larger as is also mentioned earlier. The correspondence between simulated and real currents is further confirmed by noting the relative magnitude of the emittance and perveance terms for the neutralized case, where the terms balance for the high currents. With the range simulated we thus expect to explore the regime from below to above the currents, where ion focusing becomes important. Since the simulations include plasma kinetic effects, they elucidate to what extent a beam will be space charge neutralized.

[29] Equation (2) has been solved numerically for a range of real and simulated values. The results are shown in Figure 1. Figure 1a shows the radius as a function of distance along the beam for various real currents, and Figure 1b shows the same for currents in simulations. The thick curves represent the solutions for all currents with $K = K^o$, as well as for cases of low currents for $K = K^1$. For these situations the perveance term is so small as to have no impact on the solution. Only as currents increase does the perveance term begin to influence the solution but only for charge-neutralized beams ($K = K^1$). In the simulations the magnetic field is relatively higher, and ~3.5 oscillations are shown for the cases represented by the modulation of the thick curve. Figure 1 demonstrates that the simulations also cover the transition region from low currents, where the perveance term is unimportant, to the high current region, where ion-focusing may become important.

4. Simulation Results

[30] Results for $E_b = 5$ MeV and $N^+ = 10$ are shown in Figures 2a–2d. The left panels are for injection into a vacuum, and the right panels are for injection into a plasma. Figures 2a and 2b show the beam electron position projected onto the x, y plane, and Figures 2c and 2d show the electron energy. For reference, the solutions to (2) are shown on the electron position panels for $K = K^o$ (top curve) and $K = K^1$ (bottom curve).

[31] The beam envelope modulation seen in the simulations and the analytical solutions for a nonneutralized beam are in very good agreement and mainly reflect the

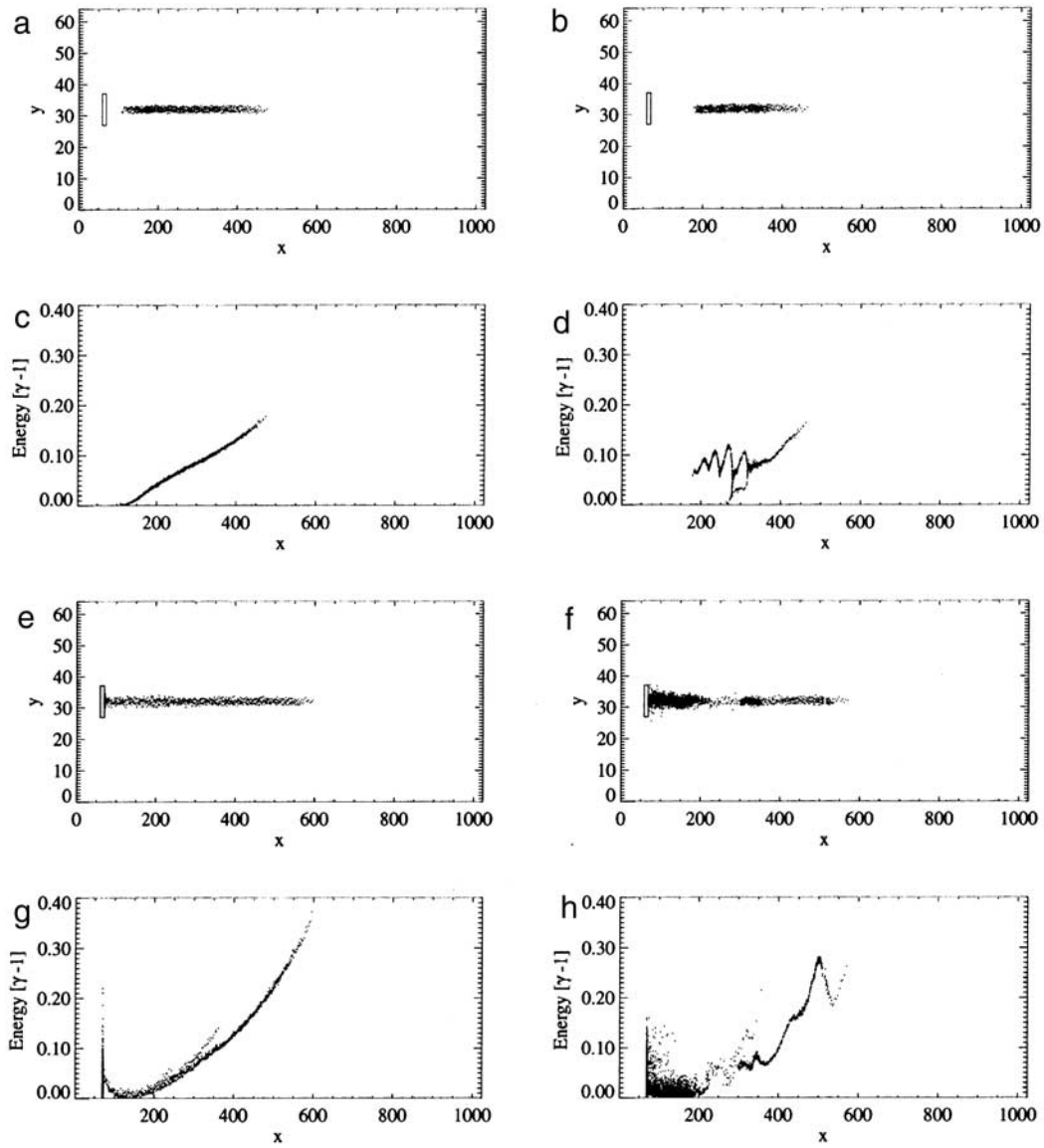

Figure 5. Electron beam with energy 50 keV injected into a (left) vacuum and (right) plasma at time $t = 1624\Delta t$. (a–d) The beam current is $N^+ = 1$, corresponding to a maximum beam density at the accelerator $n_b^o = 0.66$. (e–h) The beam current is $N^+ = 10$, corresponding to a maximum beam density at the accelerator $n_b^o = 6.6$. Other parameters are as in Figure 2.

gyration of electrons in the presence of the ambient magnetic field. The beam is slightly more confined by the plasma (Figure 2, right) relative to the vacuum case (Figure 2, left). The beam energy in the vacuum case is decreasing slightly toward the tail of the pulse, reflecting the effect of the relatively small spacecraft charging. In the plasma case the spacecraft is well neutralized, allowing beam electrons to escape with essentially the complete accelerator energy. The energy of electrons at the head of the pulse is at this point slightly modulated, primarily as a result of beam-plasma interactions.

[32] The results for high currents, with $E_b = 5$ MeV and $N^+ = 100$, are shown in Figures 2e–2h. Here the vacuum simulation (Figure 2, left) lacks the regular envelope modulation pattern of the previous simulation because spacecraft charging now becomes important. The escape energy of electrons (Figure 2g) is now seriously modulated, with decreasing energy toward the tail of the pulse. The effective mass of beam electrons is therefore decreasing toward the tail, and electrons gyrate faster. Injection into a plasma (Figure 2, right) shows strong beam-plasma interactions, which are beginning to affect the first half of the pulse, narrowing the beam envelope and generating oscillations in envelope and beam electron energy. The results indicate that while the analytical considerations point to the beam forces as instrumental in establishing conditions for beam pinching and propagation in the ion-focused regime, beam-plasma interactions dominate the propagation aspects by establishing more complicated plasma structures in the beam region, which, in turn, determines

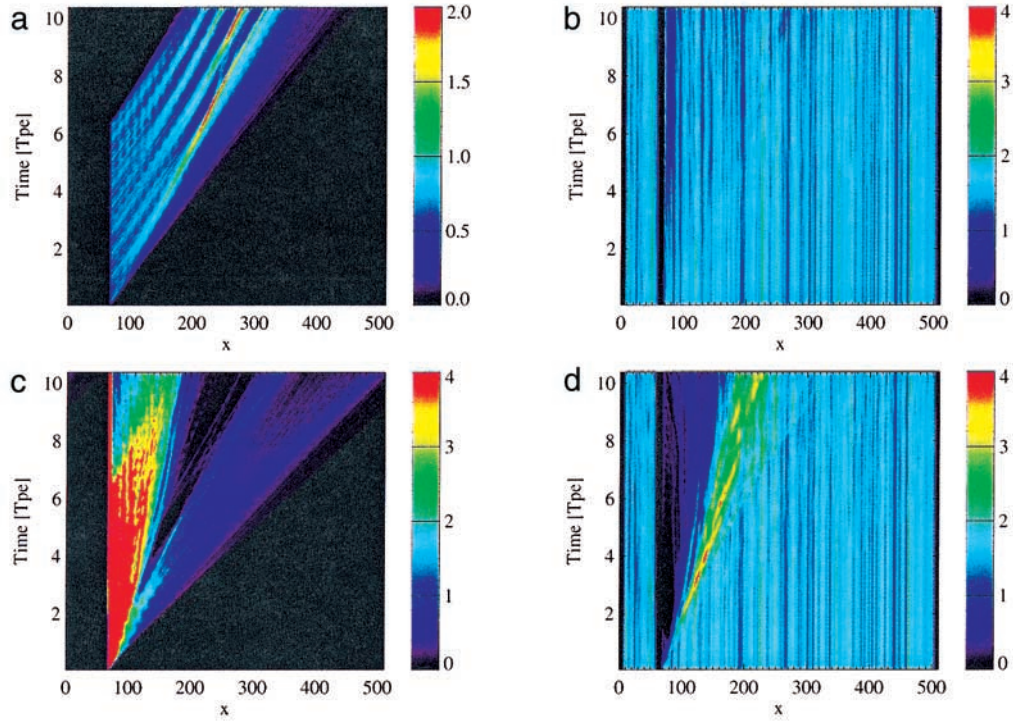

Figure 6. (a, c) Beam density and (b, d) ambient plasma density on the beam axis as a function of time and position along x. The beam energy is 50 keV. The beam currents are $N^+ = 1$ (a, b) and $N^+ = 10$ (c, d). Other parameters are as in Figure 2.

a rather complicated functional dependence of the parameter f with space and time.

[33] To study the beam-plasma interaction further, Figure 3 shows the beam and ambient densities on the beam axis as a function of position along the axis and time. In the low-current case (Figures 3a and 3b) the beam density (Figure 3a) is unaffected by the plasma and shows the expected modulation from beam electron gyration in the ambient magnetic field. The ambient density (Figure 3b) is pushed aside at the locations of beam condensation induced by beam gyration. This effect is particularly strong for the high-current case, where eventually most of the beam region is vacated by the ambient plasma. This creates the conditions for space charge-neutralized propagation where ion-focusing may become effective, and this explains the reduced beam radius in this case. The high-frequency oscillations in the front half of the pulse are possibly part of a transient stage, where a channel is being formed in the plasma, allowing later portions of the beam to propagate with much smaller energy loss.

[34] The electric fields and ambient plasma current densities in the center x, y plane are shown in Figure 4. Figures 4a–4d are the low-current case, and Figures 4e–4h are the high-current case. Plasma oscillations seen in the E_x component of the electric field are generated for both low- and high-current beams, with the higher current creating the stronger oscillations. The current along the ambient magnetic field J_x carries the return current to the spacecraft. As this current is carried by plasma electrons drifting back toward the spacecraft, the current is primarily positive but modulated by the ambient plasma oscillations. For low currents the return current maximizes in the wake of the beam close to the spacecraft, while for high currents this region is vacated by ambient electrons.

[35] The electric field perpendicular to the beam, E_y, primarily reflects the space charge modulation by the beam and the ambient plasma. It is directed toward the axis in the region of x occupied by the beam and away from the axis in the region occupied by the wake and the spacecraft. The azimuthal current J_z is carried by the $\mathbf{E} \times \mathbf{B}$ drift around the beam and therefore changes sign from the beam to the wake region. Both the azimuthal current and the electric field undergo small-scale oscillations in the beam region, with stronger oscillations for the case of higher currents. The same modulations are seen for the high-current case in the density and envelope shown in Figures 3 (envelope) and 4 (density).

[36] Turning now to keV-energy beams, results of simulations with $E_b = 50$ keV and $N^+ = 1$ are shown in Figures 5a–5d. The beam duration is the same as that in the previous simulations, and the current is smaller by a factor 10 relative to the low-current case for relativistic beams. The beam is not propagating as far into the simulation domain since $\beta = 0.44$ in this case, whereas $\beta \simeq 1$ for relativistic beams. The beam radius is smaller because the beam electron mass is smaller than that for relativistic electrons. These two effects increase the beam density relative to relativistic beams. The spacecraft charging for beam injection into a vacuum (Figure 5c) significantly influences the beam escape energy, allowing the tail of the pulse to escape with a minimum of energy. When the beam enters a plasma, strong beam-plasma

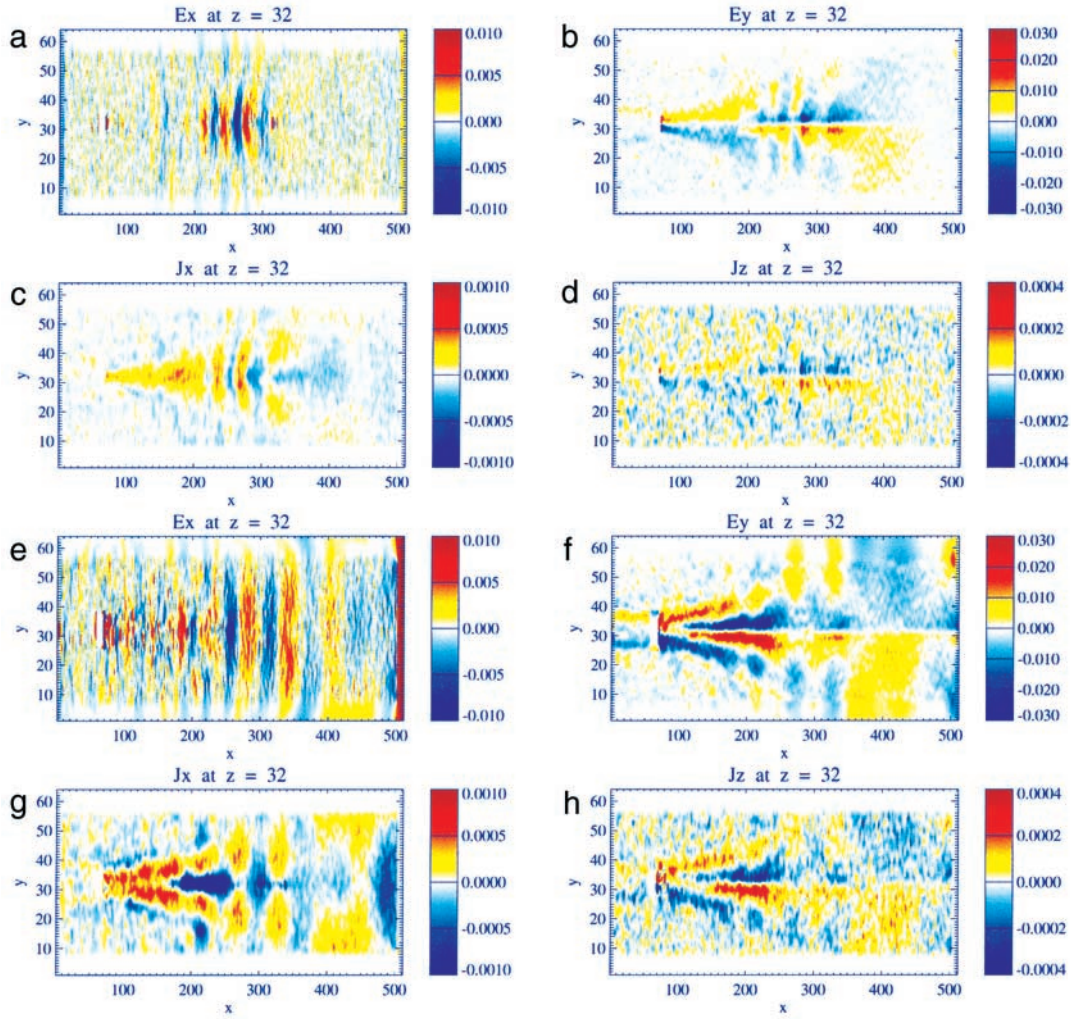

Figure 7. Electric field x, y components and ambient plasma current densities x, z components in the xy center plane at time $t = 1624\Delta t$. The beam energy is 50 keV. (a–d) $N^+ = 1$. (e–h) $N^+ = 10$. Other parameters are as in Figure 2.

interactions are generated, seriously distorting beam coherence (Figure 5d).

[37] The case of $E_b = 50$ *keV* and $N^+ = 10$ is shown in Figures 5e–5h. The current is equivalent to the low-current case of the MeV-beam simulations. For injection into a vacuum (Figures 5e and 5g) only a small fraction ($\sim$10%) escapes the spacecraft, with the front of the beam experiencing acceleration to energies well above the accelerator energy. Such acceleration is related to the formation of so-called virtual cathodes in the beam, which are regions of high negative space charge. This phenomenon is well known from past simulations [*Okuda and Ashour-Abdalla*, 1990; *Pritchett*, 1991] and is also present in the high-current case of the relativistic beam simulation shown above. The effect is thought to account for observations of transient spacecraft potentials excursions exceeding the accelerator energy [*Maehlum et al.*, 1988]. Injection into a plasma (Figures 5f and 5h) allows most of the beam electrons to leave the spacecraft structure, however, with very small energy or trapped in the spacecraft potential sheath. Again, only a smaller portion of the beam escapes with a significant fraction of the accelerator energy.

[38] The beam and plasma densities for the keV-beam simulations are shown in Figure 6. The beam density modulation for the low-current case in vacuum (Figure 6a), where the complete pulse escapes the spacecraft, shows no modulation from beam gyration in the ambient field but rather modulations from beam-plasma interactions. The ambient plasma is in this case only slightly modulated by the beam. Injection of the high-current beam shows a complete dominance of beam electrons in the region close to the spacecraft, where ambient electrons are expelled and pushed ahead of the expansion of this dense portion of the beam.

[39] The electric fields and current densities are shown in Figure 7. The most noticeable difference from the relativistic beams is the absence of the high-frequency modulations. Otherwise, the orientation of fields and currents and the generation of plasma oscillations are much the same. The E_y component for the high-current case shows the establishment of a double-layer region around

the beam close to the spacecraft. The innermost axial region is dominated by the negative charge from the beam electrons, while an outer positive space charge sheath extending from the spacecraft is enveloping the beam region.

5. Discussion

[40] Relativistic beams are found to be more stable than keV-energy beams studied in the past by particle simulations [*Okuda and Ashour-Abdalla*, 1990; *Pritchett*, 1991] and in space experiments [*Neubert and Banks*, 1992]. The enhanced stability is due to decreased beam density, a larger electron mass, and less dependence on spacecraft charging.

[41] Because of the increasing beam electron velocity with energy, the beam density decreases with energy as $1/\beta$ or $n_b \simeq \gamma/\sqrt{\gamma^2 - 1}$. The beam radius increases with relativistic electron mass, and the density is further reduced by a factor γ^2. The combined effects on the density from the increased energy is then $n_b \simeq 1/\left(\gamma\sqrt{\gamma^2 - 1}\right)$. Thus, for the same ratio of the beam to plasma densities the high-energy case allows a stronger current.

[42] The simulations presented here are for beams injected parallel to the magnetic field, where a stronger field than that encountered in the ionosphere has been applied because of limitations in the size of the computational box. The beam densities relative to ambient densities are then somewhat higher than those for the general case encountered in an experimental situation in the ionosphere. Here, keV-beams injected at some angle to the magnetic field have been observed gradually to spread with the initial beam opening angle and to begin to lose their helical structure after a few gyrations [*Neubert et al.*, 1995]. The estimates of beam density and stability presented here are therefore somewhat conservative.

[43] The increased electron mass also reduces the impact of the plasma on the beam because the beam electron momentum is larger by a factor γ. Finally, the relative importance of spacecraft charging effects on beam escape energy is reduced by the beam energy or $\gamma - 1$. In the present study, which is limited to single-pulse injections and not multiple ones anticipated in future space experiments, the spacecraft charging had little effect on relativistic pulses injected into a plasma (ionosphere).

[44] For propagation over longer distances the beam will experience scattering in both energy and pitch angle. Upward injection from the ionosphere will result in energy loss of the order of 10% or less, a number estimated for relativistic electrons injected into the magnetosphere from above thunderstorms during sprite generation [*Lehtinen et al.*, 2000]. For beam injection downward into the upper atmosphere from the ionosphere with accelerators available today, a situation of interest when studying properties of artificial upward discharges, only a small fraction of the beam energy will be lost to beam-plasma interactions.

[45] **Acknowledgments.** We are grateful for the valuable discussions held with Y. Y. Lau. The work was supported by AirForce contract F19628-93-k-003.

[46] Michel Blanc thanks George Khazanov and another referee for their assistance in evaluating this paper.

References

Banks, P. M., A. C. Fraser-Smith, B. E. Gilchrist, K. J. Harker, L. R. O. Storey, and P. R. Williamson, New concepts in ionosphere modification, *AFGL-TR-88-0133*, Air Force Geophys. Lab., Bedford, Mass., 1987.

Banks, P. M., A. C. Fraser-Smith, and B. E. Gilchrist, Ionosphere modification using relativistic electron beams, *AGARD Conf. Proc.*, *485*, 22, 1990.

Buneman, O., TRISTAN: The 3-D electromagnetic particle code, in *Computer Space Plasma Physics: Simulation Techniques and Software*, edited by H. Matsumota and Y. Omura, pp. 67–84, Terra Sci., Tokyo, 1993.

Humphries, S., Jr., *Charged Particle Beams*, Wiley-Interscience, New York, 1990.

Jost, R. J., Space borne relativistic electron accelerator system, Phase 1: Feasibility study, *PL-TR-93-2113*, Phillips Lab., Hanscom Air Force Base, Mass., 1993.

Khazanov, G. V., M. W. Liemohn, E. N. Krivorutsky, J. U. Kozyra, and B. E. Gilchrist, Interhemisphere transport of relativistic electron beams, *Geophys. Res. Lett.*, *26*, 581, 1999.

Khazanov, G. V., M. W. Liemohn, E. N. Krivorutsky, J. U. Kozyra, J. M. Albert, and B. E. Gilchrist, On the influence of the initial pitch angle distribution on relativistic electron beam dynamics, *J. Geophys. Res.*, *105*, 16,093, 2000.

Lawson, J. D., *The Physics of Charged-Particle Beams*, Oxford at the Clarendon Press, London, 1988.

Lehtinen, N. G., U. S. Inan, and T. F. Bell, Trapped energetic electron curtains produced by thunderstorm driven relativistic runaway electrons, *Geophys. Res. Lett.*, *27*, 1095, 2000.

Maehlum, B. N., J. Troim, N. C. Maynard, W. F. Denig, M. Friedrich, and K. M. Torkar, Studies of the electrical charging of the tethered electron accelerator mother-daughter rocket MAIMIK, *Geophys. Res. Lett.*, *15*, 725, 1988.

Neubert, T., and P. M. Banks, Recent results from studies of electron beam phenomena in space plasmas, *Planet. Space Sci.*, *40*, 153, 1992.

Neubert, T., and B. Gilchrist, 3D electromagnetic PIC simulations of relativistic electron pulse injections from spacecraft, *Adv. Space. Res.*, *29*(9), 1385, 2002.

Neubert, T., J. L. Burch, and S. B. Mende, The SEPAC artificial aurora, *Geophys. Res. Lett.*, *22*, 2469, 1995.

Neubert, T., B. Gilchrist, S. Wilderman, L. Habash, and H. J. Wang, Relativistic electron beam propagation in the Earth's atmosphere: Modeling results, *Geophys. Res. Lett.*, *23*, 1009, 1996.

Okuda, H., and M. Ashour-Abdalla, Injection of an overdense electron beam in space, *J. Geophys. Res.*, *95*, 24,307, 1990.

Pritchett, P. L., A three-dimensional simulation model for electron beam injection experiments in space, *J. Geophys. Res.*, *96*, 13,781, 1991.

Sentman, D. D., E. M. Wescott, D. L. Osborne, D. L. Hampton, and M. J. Heavner, Preliminary results from the Sprites94 aircraft campaign, 1, Red sprites, *Geophys. Res. Lett.*, *22*, 1205, 1995.

B. Gilchrist, Space Physics Research Laboratory, University of Michigan, Ann Arbor, MI 48109, USA.

T. Neubert, Danish Space Research Institute, Juliane Maries Vej 30, 2100 Copenhagen Ø, Denmark. (neubert@dsri.dk)